Journal of Power Sources 248 (2014) 703–713

Contents lists available at ScienceDirect

Journal of Power Sources

journal homepage: www.elsevier.com/locate/jpowsour

Analytical calculation of transfers across a cermet for solid oxide fuel cells and electrolyzers

Mikaël Dumortier [a,c,*], José Sanchez [a], Michel Keddam [b], Olivier Lacroix [c]

[a] Institut Européen des Membranes, Université de Montpellier 2, CC 047, 2 Place Eugène Bataillon, 34095 Montpellier Cedex 5, France
[b] UPMC-CNRS, Laboratoire Interfaces et Systèmes Electrochimiques, CC 133, 4 Place Jussieu, 75252 Paris Cedex 5, France
[c] AREVA NP, Centre Technique, UM2 Place Eugène Bataillon Bâtiment 13-2 étage, 34 095 Montpellier Cedex 5, France

HIGHLIGHTS

- Analytical expressions for transport quantities inside a cermet electrode.
- Dimensionless number for the prediction of the location of the reaction.
- Analytical expression of the reaction layer thickness in the electrode.

ARTICLE INFO

Article history:
Received 19 December 2012
Received in revised form
11 July 2013
Accepted 29 September 2013
Available online 12 October 2013

Keywords:
Modelling
Solid oxide cells
Cermet
Hydrogen

ABSTRACT

This work focuses on the calculation of transfers inside a cermet for solid oxide membrane fuel cells and electrolyzers. A differential system of equations presented in a previous work is linearized for low inlet current densities using assumptions that can be checked quantitatively. By integrating the linearized equations, we obtain explicit functions that allow direct calculation of the physical quantities describing the transfers of the process inside the cermet. The functions show good agreement with the values obtained with the non-linearized system. In addition, the model does not require any numerical simulation to be solved and can be implemented in common spread sheets fairly accurately. A remarkable dimensionless number, named *A*, appears in the demonstration and is used for the calculation of the reaction layer thickness of the cermet, where 99.9% of the charge transfer occurs. This thickness does not depend on inlet current density or on the thickness of the cermet.

1. Introduction

Different technologies are currently being studied for hydrogen production with low carbon dioxide emissions. Among these technologies, electrolysis of water at low temperature using polymer membranes and noble metals has already been extensively investigated on an industrial scale. This electrically driven process can also been carried out at high temperature with inorganic membranes. The latter process presents several advantages compared to low temperature electrolysis, i.e. decreased electrical power consumption, the electrodes can be made without using expensive noble metals and the heat that is required for the process can be supplied by nuclear reactors, which limits greenhouse gas production [1].

Among the high temperature electrolysis processes, solid oxide technology has been widely described in the literature. The process can either be run at high (800–1000 °C), intermediate (600–800 °C) or low temperatures (400°C–600 °C). At high and intermediate temperature, the solid oxide conducts oxygen electrons and the process is less electricity-consuming compared to the low temperature process, but the hydrogen produced needs to be separated from steam. At low temperature, the solid oxide can conduct protons [2], which means the hydrogen produced at the cathode is pure and a subsequent separation step can be avoided (Fig. 1). In addition, the lower temperature process contributes to the long-term resistance of materials.

In high temperature electrolysis, the cell is an electrochemical membrane reactor composed of two channels separated by a dense solid oxide layer between two porous electrodes. In proton conducting cells, steam is fed at the anode and oxidized in the cermet, which is a mixed media made of metal and ceramic. Mathematical modelling of such devices helps understanding the phenomena inside the cells and makes it easier to predict their operation.

* Corresponding author. Institut Européen des Membranes, Université de Montpellier 2, CC 047, 2 Place Eugène Bataillon, 34095 Montpellier Cedex 5, France. Tel.: +33 46714929; fax: +33 467149235.
E-mail address: mikael.dumortier@gmail.com (M. Dumortier).

0378-7753/$ – see front matter © 2013 Elsevier B.V. All rights reserved.
http://dx.doi.org/10.1016/j.jpowsour.2013.09.142

Nomenclature

A	transfer current density distribution number (dimensionless)
C_T	total concentration (mol m^{-3})
D_i	diffusion coefficient for species i (m^2 s^{-1})
$D_{i,Kn}^{eff}$	effective Knudsen diffusion coefficient for species i (m^2 s^{-1})
D_{ij}^{eff}	effective binary diffusion coefficient for species i and j (m^2 s^{-1})
$\vec{e}_x$	unitary vector directed to the thickness of the electrode (dimensionless)
F	Faraday constant (C mol^{-1})
I	inlet intensity (A)
i_r	volumetric transfer current (A m^{-3})
i_r^0	exchange current density (A m^{-3})
$\vec{j}_i$	charge flux density inside phase i (A m^{-2})
J_0	inlet electrical current density (A m^{-2})
k	charge of the ion conducted by the ceramic phase
K	electrochemical transfer number (dimensionless)
L	electrode thickness (m)
L_{reac}	reaction layer thickness (m)
M_i	molar weight for species i (kg mol^{-1})
M_I	molar weight of the transported ion (kg mol^{-1})
$\vec{N}_i$	molar flux density for species i (mol s^{-1} m^{-2})
P	total pressure (Pa)
Pe	Peclet number (dimensionless)
Q	volumetric flow rate (m^3 s^{-1})
R	ideal gas constant (J mol^{-1} K^{-1})
r_i	grain radius inside phase i (m)
r_r	total volumetric molar transfer rate (mol s^{-1} m^{-3})
s_i	surface fraction for phase i (dimensionless)
T	local uniform temperature (K)
$\vec{u}$	velocity vector (m s^{-1})
X	arbitrary physical quantity
X^+	reference added concentration factor (dimensionless)
x	position across the electrode (m)
x_i	molar fraction for species i (dimensionless)
x_{ox}, x_{red}	molar fraction for the oxidizer and the reducer (dimensionless)
α	charge transfer coefficient (dimensionless)
ε_i	volumetric fraction of the phase i (dimensionless)
η	overpotential (V)
ν_i	stoichiometric coefficient for species i (dimensionless)
ρ_g	gas density (kg m^{-3})
σ_i	electrical conductivity for phase i (S m^{-1})
ϕ_i	charge potential inside phase i (V)
σ_{red}	ceramic conductivity fraction (dimensionless)

Numerical analysis

∇	del operator
Δ	change of variable quantity
d	differential operator
∂	partial differential operator

Indexes and subscripts

e	variable attached to the metallic phase or to charge carried by electrons
ext	used for surfaces included in the boundary of the control volume
eff	effective value of a variable
g	variable attached to the gas phase
io	variable attached to the ceramic phase or to charge carried by ions
int	used for surfaces inside the control volume
TP	variable attached to the triple phase boundary
*	dimensionless quantity
0	reference quantity

Abbreviations

PDE	partial differential equation
SOEC	solid oxide electrolysis cell
SOFC	solid oxide fuel cell

Fortunately for modellers, the equations describing transport phenomena inside solid oxide fuel cells (SOFC) and solid oxide electrolysis cell (SOEC) are the same, as one technology is the reverse functioning of the other. Therefore many numerical models are valid for both technologies. While complex 3D models have been developed to describe transfers in high temperature fuel cells or electrolyzers [3–15], only few have integrated models available for the non-code user. In 2007, Meng Ni proposed a 1D analytical model to predict the potential inside a solid oxide electrolysis cell (SOEC) without numerical solving [16]. The model is based on the assumption that the electrochemical reaction is confined to a thin layer; in a previous work, our group demonstrated that the assumption is only valid under certain conditions [17], i.e. low ionic conductivity of ceramics, no limitation in the diffusion of species inside the electrode, metal grain radius not too large compared to the ceramic grain radius. However, these statements are only qualitative. The objective of this paper is to provide a model featuring analytical expressions of the physical quantities inside a cermet electrode used in solid oxide cells, assuming that the electrochemical reaction can occur anywhere in the cermet. The model is derived from a comprehensive 3D model which has been simplified with two major hypotheses: unidirectional transport phenomena and linearized Butler–Volmer equation. The frames in which those assumptions are valid are also developed in this study. The model does not require any numerical simulation to be solved and can be implemented in common spread sheets fairly accurately. In order to be the most general possible, the model equations are written in dimensionless form. The undimensionalization of the governing equations for transfer inside a fuel cell has already been investigated by Gyenge in 2005 [18]. However to our knowledge, no integration of a linearized system of equations has ever been investigated to predict the value of the physical quantities along a porous electrode.

2. Modelling

In this study, the electrodes considered are cermets, which are among the most interesting candidates as electrode material for high-temperature steam electrolysis [2]. A cermet is a mixed porous media comprising three phases: a metallic phase which conducts electrons, a ceramic phase which conducts protons and a gas phase constituted by the porosity where reactants and products of the electrochemical reaction are conveyed (Fig. 2).

While charge is transported by migration in solid phases, chemical species are transported in gas by diffusion and convection. These transport phenomena inside electrodes have been mathematically modelled in a previous work [17] using continuity equations obtained by applying the volume averaging method [19]

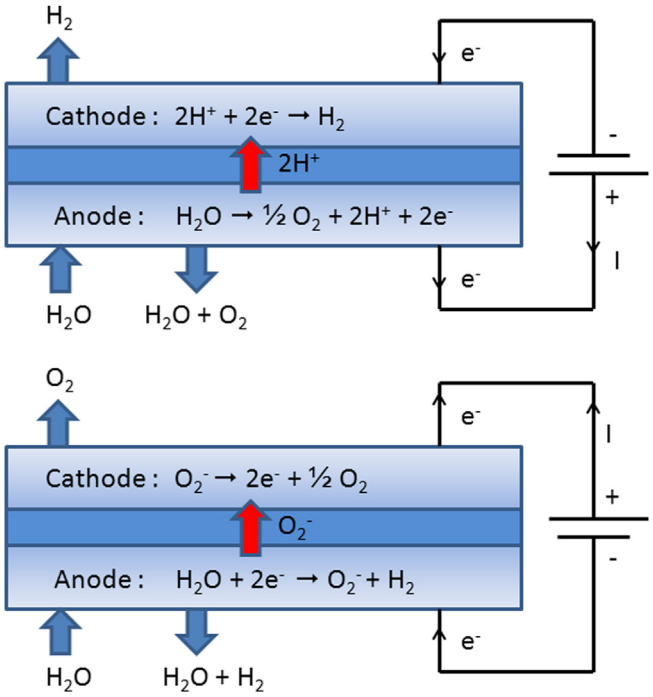

Fig. 1. Principle of proton and anion conducting SOECs.

to a representative volume of electrode. As explained earlier, this paper focuses on the establishment of a 1D model derived from these continuity equations.

2.1. Assumption 1: one dimensional model

The transport phenomena are represented by partial differential equations (PDE). A PDE for the function $u(x,y,z)$ is an equation of the form :

$$F\left(x, y, z, u, \frac{\partial u}{\partial x}, \frac{\partial u}{\partial y} \cdots \frac{\partial^2 u}{\partial y \partial z} \cdots \frac{\partial^2 u}{\partial z^2}\right) = 0 \tag{1}$$

A PDE often requires numerical simulation in order to be solved. However, using this effective calculation strategy gives the values of $u(x,y,z)$ but not the expression of the function itself. One aim of this work was to find assumptions that can be realistically considered regarding the behaviour of the system to reduce those PDE to a simpler form.

$$F(x, u) = 0 \tag{2}$$

To obtain the functions, we assumed that the different quantities vary along a single direction x, oriented by the electric current path across the electrode (Fig 3). Here, the direction is assumed to

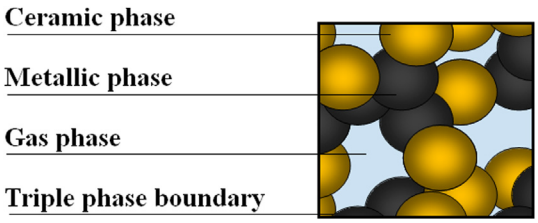

Fig. 2. The cermet medium and its different phases.

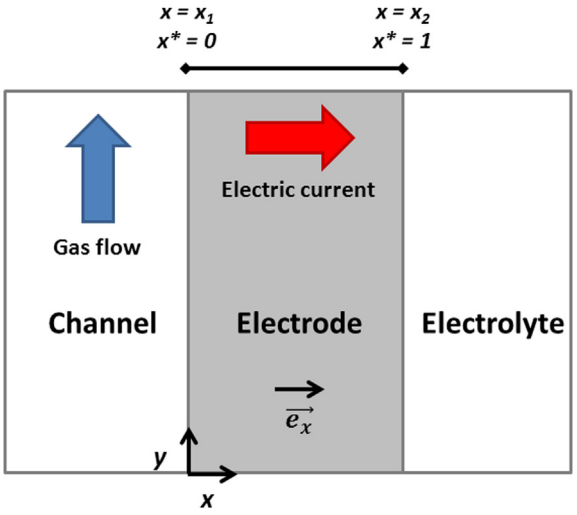

Fig. 3. Formal representation of the electrolyser.

be perpendicular to the electrode. As a result, the divergence operator and the gradient operator can be simplified as follows:

$$\nabla . = \frac{\partial}{\partial x} \quad \vec{\nabla} = \frac{\partial}{\partial x}\vec{e}_x \tag{3}$$

Different conditions are required to validate this assumption. First of all, the electric current must be quite homogeneous along the y direction of the cermet. This statement presumes that the distribution of the metallic and ceramic phases along the y direction is homogeneous. The quantities can however vary across the x direction of the electrode.

Secondly, during the electrochemical process, the mixture in the anode channel is enriched in oxygen or hydrogen depending on the type of membrane reactor, i.e. a fuel cell or electrolyser. If the flow is crosswise to the electrode, the variation of molar fractions in the channel in the y direction can have an impact on the transport phenomena in the cermet. With a simple analysis, the changes in molar fractions inside the channel can be established through Equation (4). In this work we believe that the 1D assumption can be reasonably considered valid if the variations are lower than 10%.

$$\Delta x_i \approx \frac{\mathrm{RTI}}{\mathrm{PQF}} \frac{\nu_i}{\nu_{e-}} \ll 0.1 \tag{4}$$

Taking into consideration this assumption, the analytical expressions of the variables of the system can be obtained.

2.2. Current densities and potentials

In a cermet, electrons are transported by the metal and ions by the ceramic. The behaviour of this transport is represented by Ohm's law:

$$\text{For the ceramic} : j_{io} = -\sigma_{io}\frac{\partial \phi_{io}}{\partial x} \tag{5}$$

$$\text{For the metal} : j_{e} = -\sigma_{e}\frac{\partial \phi_{e}}{\partial x} \tag{6}$$

The transport number of charged species inside the ceramic is supposed equal to 1, meaning that only one ion is conveyed in the ceramic, hence mixed-conducting ceramics are not studied here. During the electrochemical reaction, charge is transferred from the

metal to the ceramic. The rate of this transfer is calculated using the Butler–Volmer equation [17]:

$$i_r = i_r^0\left[\frac{x_{red}}{x_{red}^0}\exp\left(\frac{\alpha\nu_e F}{RT}\eta\right) - \frac{x_{ox}}{x_{ox}^0}\exp\left(\frac{-\alpha\nu_e F}{RT}\eta\right)\right] \quad (7)$$

The overpotential, η, corresponds to the difference of electrical state between the two solid phases:

$$\eta = (\phi_e - \phi_{io}) - \left(\phi_e^0 - \phi_{io}^0\right) \quad (8)$$

The reference electric potential, ϕ_e^0, is calculated with the Gibbs energy of the electrochemical reaction and the reference ionic potential, ϕ_{io}^0, is set to 0.

As charge passes from a medium to another, the value of the currents varies with the intensity of the charge transfer density, i_r. The variables are interconnected through the charge conservation expressions:

$$\text{For the ceramic}: \frac{\partial}{\partial x}(j_{io}s_{io}) = \nu_e i_r \varepsilon_{TP} \quad (9)$$

$$\text{For the metal}: \frac{\partial}{\partial x}(j_e s_e) = -\nu_e i_r \varepsilon_{TP} \quad (10)$$

Finally, current conservation inside the phases is expressed by the equation below:

$$j_{io}s_{io} + j_e s_e = J_0 \quad (11)$$

2.3. Assumption 2: low currents and overpotentials

This equation system cannot be solved analytically because of the non-linearity of the Butler–Volmer equation. However, the exponential terms of the equation can be linearized by a first order Taylor development at 0 as follows:

$$e^x = 1 + x + o(x) \quad (12)$$

This assumption is valid for low overpotential or low current densities:

$$\frac{\alpha\nu_e F}{RT}\eta \ll 1 \quad (13)$$

$$\frac{J_0}{i_r^0 \varepsilon_{TP} L} \ll 1 \quad (14)$$

Note that Equation (13) states that a current is considered to be low when it is much smaller than the exchange current density of the electrode, i.e. when the system is close to the thermodynamical equilibrium. Using Equation (4), the variation of the molar fractions of species with x is also supposed to be negligible compared to the variation of the overpotential. Therefore Equation (7) reduces to:

$$i_r = i_r^0\frac{\alpha\nu_e F}{RT}\eta\left(\frac{x_{red}}{x_{red}^0} + \frac{x_{ox}}{x_{ox}^0}\right) \quad (15)$$

2.4. Undimensionalization of the system

Once these assumptions are made, the equations can be written in dimensionless form. The process of undimensionalization consists in making a change of variables in equations so that the new variables and their derivatives are of the same order of magnitude. It facilitates the manipulation of equations during calculations, helps in the comparison of the different terms, and can also be used to recover characteristic properties of the system such as length, time constants and dimensionless numbers. The new variables are expressed as the ratio of the variables to a relevant order of magnitude, as in this example:

$$X^* = X/X_0 \quad (16)$$

The reference value depends on the parameters of the process, and is not affected by derivation:

$$d_{x^*}X^* = \frac{\partial X^*}{\partial x^*} = \frac{x_0}{X_0}\frac{\partial X}{\partial x} \quad (17)$$

Reference values are obvious for position and current densities:

$$x^* = x/L \quad (18)$$

$$i_r^* = i_r/i_r^0 \quad (19)$$

$$j_e^* = j_e s_e/J_0 \quad (20)$$

$$j_{io}^* = j_{io}s_{io}/J_0 \quad (21)$$

The reference values for overpotentials are deduced from Butler–Volmer equation:

$$\eta^* = \eta/\eta_0 \quad (22)$$

$$\eta_0 = RT/\alpha\nu_e F \quad (23)$$

The dimensionless forms of Equations (5)–(11) are written as follows:

$$j_{io}^* = -(s_{io}\sigma_{io}/\sigma_0)d_{x^*}\phi_{io}^* \quad (24)$$

$$j_e^* = -(s_e\sigma_e/\sigma_0)d_{x^*}\phi_e^* \quad (25)$$

$$i_r^* = X^+\eta^* \quad (26)$$

$$d_{x^*}j_e^* = -Ki_r^* \quad (27)$$

$$d_{x^*}j_{io}^* = Ki_r^* \quad (28)$$

$$j_e^* + j_{io}^* = 1 \quad (29)$$

with

$$X^+ = x_{red}/x_{red}^0 + x_{ox}/x_{ox}^0 \quad (30)$$

$$\sigma_0 = J_0 L/\eta_0 \quad (31)$$

$$K = L\nu_e i_r^0 \varepsilon_{TP}/J_0 \quad (32)$$

Coupling the Butler–Volmer equation (26) with the continuity equation for charge ((27)–(28)) and current conservation (29) gives a second order differential equation verified by the ionic charge current:

$$d_x^2 j_{io}^* - Aj_{io}^* = \sigma_{red} \quad (33)$$

$$\text{with } \sigma_{red} = \frac{s_{io}\sigma_{io}}{s_{io}\sigma_{io} + s_e\sigma_e} \quad (34)$$

$$A = \frac{L^2 \nu_e{}^2 i_r^0 \varepsilon_{TP} \alpha F}{RT} \left(\frac{x_{red}}{x_{red}^0} + \frac{x_{ox}}{x_{ox}^0} \right) \left(\frac{1}{s_{io}\sigma_{io}} + \frac{1}{s_e \sigma_e} \right) \quad (35)$$

The boundary conditions for the ionic current are given by:

$$\text{No ionic current at the electrode/channel interface} : j_{io}^*(0) = 0 \quad (36)$$

$$\text{At the electrolyte/electrode interface the current is purely ionic} : j_{io}^*(1) = 1 \quad (37)$$

The solution of this differential system composed of Equations (33), (36) and (37) is:

$$j_{io}^*\left(x^*\right) = \sigma_{red}\left(1 + f^+\left(x^*\right) - f^-\left(x^*\right)\right) \quad (38)$$

with

$$f^+\left(x^*\right) = D_e \exp\left(\sqrt{A}x^*\right) \quad (39)$$

$$f^-\left(x^*\right) = (D_e + 1)\exp\left(-\sqrt{A}x^*\right) \quad (40)$$

$$D_e = \frac{\frac{s_e \sigma_e}{s_{io}\sigma_{io}} + \exp\left(-\sqrt{A}\right)}{\exp\left(\sqrt{A}\right) - \exp\left(-\sqrt{A}\right)} \quad (41)$$

From Equations (29) and (38), the expression of dimensionless electrical current is obtained:

$$j_e^*\left(x^*\right) = 1 - \sigma_{red}\left(1 + f^+\left(x^*\right) - f^-\left(x^*\right)\right) \quad (42)$$

By derivation of this quantity, and coupling it with Equation (27), the expression of the exchange current density in dimensionless form is given by:

$$i_r^* = \frac{\sqrt{A}}{K}\sigma_{red}\left(f^+\left(x^*\right) + f^-\left(x^*\right)\right) \quad (43)$$

Hence, the dimensionless overpotential using Equation (26) can be written as follows:

$$\eta^* = \frac{\sqrt{A}}{KX^+}\sigma_{red}\left(f^+\left(x^*\right) + f^-\left(x^*\right)\right) \quad (44)$$

2.5. Mass transfer

The chemical species needed for the electrochemical reactions are transported to the triple phase boundary in the porous electrode. The model chosen for mass transport inside solid oxide cells is the Dusty Gas Model, as recommended by Suwanwarangkul et al. [4]. For two species, we have shown in our previous work [17] that the Dusty Gas model can be expressed as follows:

$$N_i = -D_i \frac{\partial x_i}{\partial x} C_T + x_i u \quad (45)$$

with

$$D_i = \frac{D_{i,Kn}^{eff} D_{ij}^{eff}}{D_{ij}^{eff} + x_j D_{i,Kn}^{eff} + x_i D_{j,Kn}^{eff}} \quad (46)$$

Reducing this equation to its dimensionless form gives:

$$N_i^* = -d_{x^*} x_i / Pe_i + u^* x_i \quad (47)$$

With

$$N_i^* = \frac{N_{ix} s_g}{N_i^0} \quad (48)$$

$$u^* = x_i C_T u / N_i^0 \quad (49)$$

$$N_i^0 = \frac{J_0}{F}\frac{\nu_i}{\nu_e} \quad (50)$$

$$Pe_i = \frac{L N_i^0}{C_T D_i} = \frac{RT}{P}\frac{J_0 L}{F D_i}\frac{\nu_i}{\nu_e} \quad (51)$$

Pe_i is the Peclet number for species i. It compares advection and diffusion effects in mass transfer. If $Pe_i << 1$, then transport of chemical species inside the medium occurs by diffusion while if $Pe_i >> 1$, then mass transfer is governed by advection.

In this work, the Peclet number is supposed to be very small in the electrodes. In the problem presented in Section 3, the Peclet number of oxygen inside the porous anode for a proton conducting SOEC is equal to $Pe_{O2} = 2.8 \times 10^{-3}$ ($Pe_{H2} = 1.7 \times 10^{-2}$ in the cathode). This reasonably implies that the velocity inside the electrode is low and that the chemical species are transported by diffusion inside the cermet. Hence, Equation (47) can be written as follows:

$$N_i^* = -d_{x^*} x_i / Pe_i \quad (52)$$

In addition, chemical species are either consumed or produced inside the porous electrodes. Therefore their fluxes depend on the intensity of the electrochemical reaction. The interconnection between the phenomena is given by mass conservation for the species:

$$\frac{\partial}{\partial x}\left(s_g N_i\right) = \nu_i i_r F \varepsilon_{TP} \quad (53)$$

the dimensionless form of the equation above can be written as:

$$d_{x^*} N_i^* = K i_r^* \quad (54)$$

Similarities can be noted between dimensionless Equations (28) and (54). This shows that charge and mass conservation exhibit the same physical behaviour. This is consistent with the fact that the transport of those quantities are driven and bounded together by the electrochemical transfer.

The molar flux density, N_i, is obtained through integration of (54). Hence, boundary conditions are required. At the electrode/electrolyte interface, the molar flux of species is equal to zero as they cannot cross the electrolyte. This gives the condition:

$$N_i^*(1) = 0 \quad (55)$$

At the electrode/channel interface, the molar flux of the species i is equal to the total source of the species in the cermet.

The mass transport variables can be then calculated from the integration of Equations (52) and (54):

$$N_i^*\left(x^*\right) = -j_e^*\left(x^*\right) \quad (56)$$

$$\Delta x_i\left(x^*\right) = Pe_i\left(x^* - \sigma_{red}\left(x^* + \left(f^+\left(x^*\right) + f^-\left(x^*\right) - 2D_e - 1\right)\Big/\sqrt{A}\right)\right) \quad (57)$$

2.6. Additional assumption and physical meaning of the A number

In most cases, electrical conductivity of metals ranges between 10^3 et 10^5 S m^{-1}. These values are at least 100 times higher than the ionic conductivity of ceramics [20–22]. Hence $s_e\sigma_e >> s_{io}\sigma_{io}$. When this assumption is injected into the previous equations, they simplify into much simpler expressions and exhibit a strong dependence on the A number:

$$j_{io}^*\left(x^*\right) = \frac{\mathrm{sh}\left(\sqrt{A}x^*\right)}{\mathrm{sh}\left(\sqrt{A}\right)} \tag{58}$$

$$j_e^*\left(x^*\right) = 1 - \frac{\mathrm{sh}\left(\sqrt{A}x^*\right)}{\mathrm{sh}\left(\sqrt{A}\right)} \tag{59}$$

$$i_r^* = \frac{\sqrt{A}}{K}\frac{\mathrm{ch}\left(\sqrt{A}x^*\right)}{\mathrm{sh}\left(\sqrt{A}\right)} \tag{60}$$

$$\Delta x_i\left(x^*\right) = Pe_i\left(x^* - \frac{1}{\sqrt{A}}\frac{\mathrm{ch}\left(\sqrt{A}x^*\right)-1}{\mathrm{sh}\left(\sqrt{A}\right)}\right) \tag{61}$$

The equations show that the A number is a key dimensionless number describing the distribution of the electrochemical reaction inside the electrode. Equation (35) shows which process and structural parameters are involved into the calculation of A, therefore parametric analysis to study the influence of parameters on the quantities related to the electrochemical reaction can easily be made. To our knowledge, this dimensionless number has never been described in the literature. The number compares two limiting effects that determine the location of charge transfer:

- The cermet resistance to charge transfer, which depends on the microstructure, gas composition, electrode thickness and exchange current density. Electrochemical transfer conductivity of the electrode, σ_{th}, is the characteristic conductivity of the electrode for the electrochemical transfer.
- Charge conduction resistance inside the metal and the ceramic. When charge is transported inside the conductors, it generates energy loss because of resistance effects. The effects are represented in the A number by the conductivity σ_{OHM}, which is the harmonic mean of the conductivities of the two charge conductors.

$$A = \frac{\sigma_{th}}{\sigma_{OHM}} \tag{62}$$

$$\sigma_{th} = \frac{L^2\nu_e^2 i_r^0 \varepsilon_{TP}\alpha F}{RT}\left(\frac{x_{red}}{x_{red}^0} + \frac{x_{ox}}{x_{ox}^0}\right) \tag{63}$$

$$\frac{1}{\sigma_{OHM}} = \frac{1}{s_{io}\sigma_{io}} + \frac{1}{s_e\sigma_e} \tag{64}$$

As shown in Fig 4, when charge conduction transport is limiting, then $\sigma_{th} >> \sigma_{OHM}$ and $A >> 1$, and the reaction occurs mostly at the anode/electrolyte interface. This is consistent with our previous observations [17], in which we noted that when ceramic conductivity is low, charge transfer occurs close to the electrolyte in order to minimize the path of protons through the ceramic.

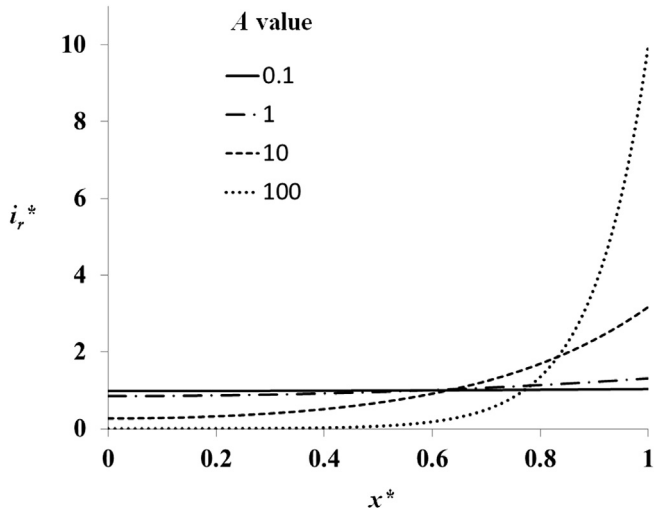

Fig. 4. Dimensionless transfer current density for several values of A. *X*-axis: dimensionless position in the cermet. *Y*-axis: dimensionless transfer current density.

When electrochemical transfer is limiting, i.e $\sigma_{th} << \sigma_{OHM}$ and $A << 1$, the reaction tends to follow the distribution of σ_{th} across the electrode. Here, σ_{th} is homogenous across the electrode, but the profile would be different, for example, in the case of graded composition electrodes [6,23–25].

The distributions of transport fluxes and transfer fluxes across the electrodes only depend on A. Equations (62)–(64) show how the parameters of the process influence those distributions. For example, inlet current density does not have any effect on the distributions, contrary to the number of electrons exchanged in the electrochemical transfer. From the expression of A, we can conclude that distribution of the electrochemical reaction across the electrode depends mainly on the reaction involved, on conductivities and on the electrode microstructure, which again, is consistent with previous observations [17].

2.7. Dimensional expressions

Dimensional expressions are required to find real values on a real electrode. Dimensional expressions are obtained from corresponding dimensionless expressions with the relationships presented below:

$$x = x^*(x_1 - x_2) + x_1 \tag{65}$$

$$X(x) = X_0X^*\left(x^*\right) = X_0X^*((x - x_1)/(x_1 - x_2)) \tag{66}$$

x_1 and x_2 are the x coordinates of the channel/electrode interface and electrode/electrolyte interface respectively. The expressions are used for the comparison between the 1D model presented in Section 2.3 and the 3D complete model presented in Section 2.1.

3. Comparison between 1D and 3D models

3.1. Calculation set up

In a previous study [17], the 3D model results were presented as a planar co-flow proton conducting SOEC (see Fig. 3) using the COMSOL Multyphysics 4.2 software. The study showed that distribution of the electrochemical reaction across the cermet depends on several parameters such as ionic conductivity and electrode microstructure. These results will be used as a basis to test the

simplified model presented here, considering the same reactor dimensions (Table 1) and boundary conditions (Table 2), parameters and reference values used in our previous work. Unless another value for the parameters is specified, the default values taken for any calculation are those presented in Table 3. In order to facilitate reading, the model developed in the previous work will be referred to as the "3D model" whereas the model developed in this work will be referred to as the "1D model". The formulae presented in Section 2.3 are expressed in dimensional form according to the geometry presented in Fig. 5.

Transfer current density, $i_r\varepsilon_{TBP}$, is proportional to the charge transferred at the triple phase boundary and to the production and consumption rate of the chemical species. Therefore, it is connected to the location where the electrochemical reaction occurs in the electrode. The integral of this quantity is fixed by the inlet current density value. Therefore other parameters can only have an effect on its distribution across the electrode. Transfer current density is thus the best suited quantity for this study and for a parametric analysis. The two models are therefore compared in terms of their prediction of transfer current density, and also in terms of their prediction of the overpotential, η, and the oxygen molar fraction, x_{O2}. With the latter two quantities, the differences between both models should appear more evidently, as they are less constrained than $i_r\varepsilon_{TP}$.

The specific reactive volume ε_{TP} can either be determined experimentally of calculated. Several models can be found in literature to relate this volume to the structural parameters of the electrode [26,27]. Correlations for the calculation of binary and Knudsen diffusion coefficient can be obtained from the well-known works of Bird et al. and Poling et al. [28,29]. Before running the calculations for the comparison, one has to check whether the assumptions for the 1D model are satisfied. As the maximum current density in this study is quite high (10,000 A m^{-2}), the linearization of the Butler Volmer equation in the 1D model could be questioned. Yet, from the values for the exchange current density and the specific reactive volume from the previous study, the low current assumption presented in Equation (13) is verified for the reference values:

$$\frac{J_0}{i_r^0\varepsilon_{TP}L} = 0.15 \tag{67}$$

The length of the cell (1 mm) is below the usual length found in literature. In fact, the priority of this comparison is not to represent real system but to test the 1D model in a cell where the assumptions explained above are satisfied. Therefore, the length of the cell was purposely kept low to reduce calculation cost and satisfy the 1D assumption presented in Equation (12). From the parameters of Tables 1 and 2, the 1D assumption is verified for every species:

$$\frac{RTI}{PQF}\frac{\nu_i}{\nu_{e-}} < 0.019 \tag{68}$$

Table 1
Reactor dimensions.

Parameter	Value
Anodic channel thickness	4×10^{-4} m
Anodic cermet thickness	1.5×10^{-4} m–5×10^{-4} m
Electrolyte thickness	1×10^{-4} m
Cathodic cermet thickness	1.5×10^{-4} m–5×10^{-4} m
Cathodic channel thickness	4×10^{-4} m
Anodic cermet length	10^{-3} m
Electrolyte length	10^{-3} m
Cathodic cermet length	10^{-3} m
Anodic channel length	1.8×10^{-3} m
Cathodic channel length	1.8×10^{-3} m

Table 2
Boundary conditions.

Boundary	Species transport	Momentum transport	Charge transport
1	Zero flux	Wall – no slip	–
2	Inflow – concentration	Velocity inlet	–
3	Outflow	Outlet – pressure	–
4	Zero flux	Wall – no slip	–
5	–	–	Ionic: zero flux electronic:flux
6,8,10,11, 13,14	Zero flux	Wall – no slip	Zero flux
7,9,12,15	Zero flux	Wall – no slip	–
16	Outflow	Outlet – pressure	–
17	–	–	Ionic:zero flux electronic:Flux
18	Zero flux	Wall – no slip	–
19	Inflow – concentration	Velocity inlet	–
20	Zero flux	Wall – no slip	–

A higher length results in higher intensities I for the same inlet current density.

3.2. Parametric results

The two models were firstly compared with the reference values given in Table 3 and then for different conductivity ratios. In both cases, comparison between the 1D and the 3D models showed a perfect match for $i_r\varepsilon_{TP}$ (see Figs. 6 and 7).

A good agreement was also achieved for prediction of the oxygen molar fraction, x_{O2}, and the overpotential, η. The results presented in Figs. 8 and 9 show that the 1D model tends to slightly underestimate the value of the overpotential when its value is low. This corresponds to the effect of the term $(x_{red}/x_{red}^0 - x_{ox}/x_{ox}^0)$ which was neglected in Section 2.2 in order to analytically solve Equation (33). The influence of this term becomes important when the overpotential is low. The values of oxygen molar fraction across the cermet are plotted in Figs. 10 and 11. Again the 1D model perfectly matches the 3D model except when the ratio between the charge conductivities of the ceramic and the metal is low.

In addition to comparing the two models, the results show that when the ratio between the conductivities is high, the electrochemical reaction occurs in an area close to the electrolyte. This phenomenon has been explained in our previous work [17]: the profile adapts in order to minimize the path of protons through the ceramic to lower ohmic losses.

The results obtained on comparison of the two models for other parameters (grain ratio radii, initial oxygen molar fraction, inlet current density) are not presented here as they can be described in

Table 3
Values of variable parameters and inlet parameters for the reference calculation.

Parameter	Reference value	Unit	Other values tested
Inlet current density	10,000	A m^{-2}	1–1000
Ionic conductivity (ceramic)	1	S m^{-1}	–
Electronic conductivity (metal)	1000	S m^{-1}	1–100,000
Particle radius (metal)	10^{-6}	m	5×10^{-7}–5×10^{-6} –2.5×10^{-5}
Particle radius (ceramic)	5×10^{-7}	m	–
Initial oxygen molar fraction	0.01	–	0.1, 0.3, 0.5, 0.9
Operating pressure	10^6	Pa	–
Operating temperature	873	K	–

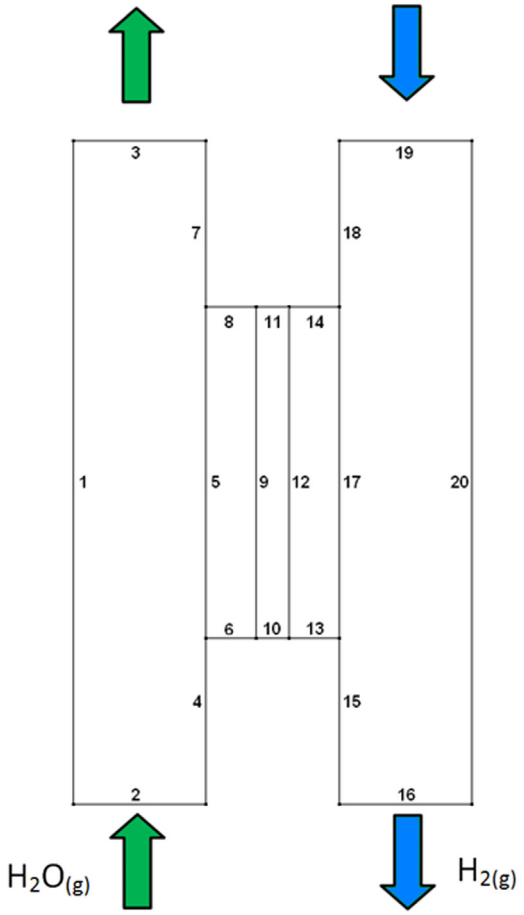

Fig. 5. Geometry used for the calculations and boundary conditions.

similar terms: perfect match for $i_r\varepsilon_{TP}$ and x_{O2}, small difference for η. In addition, we have noted that the difference between the models for η decreases with lower inlet current density. However, additional calculations showed that the 1D model deviates from the 3D model when the low current assumption (Equation (13)) is no longer valid. Therefore we can highlight the fact that the frame of the 1D model is restricted to low currents.

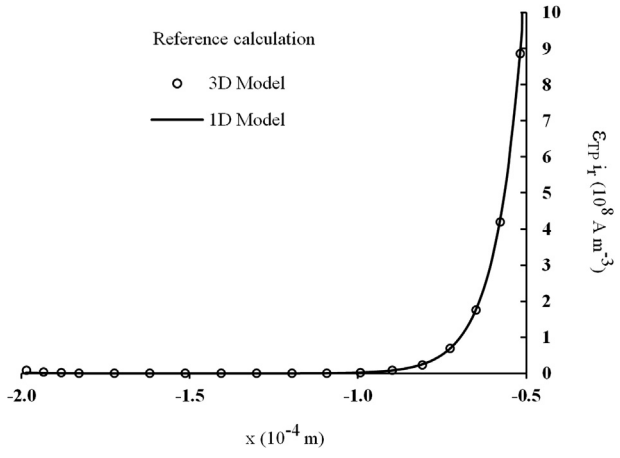

Fig. 6. Comparison between the two models on transfer current density along the anodic cermet for the reference case. *X*-axis: position in the anodic cermet (on the left the anodic channel, on the right the electrolyte). *Y*-axis: transfer current density multiplied by the specific reactive volume.

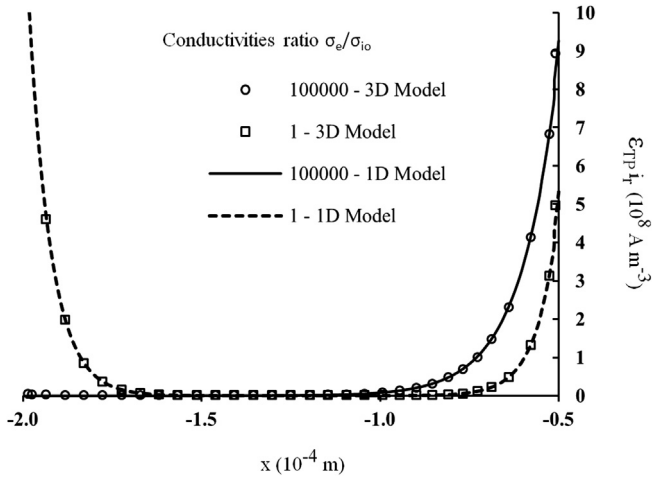

Fig. 7. Comparison between the two models on transfer current density along the anodic cermet for different conductivities ratios. *X*-axis: position in the anodic cermet (on the left the anodic channel, on the right the electrolyte). *Y*-axis: transfer current density multiplied by the specific reactive volume.

3.3. Reaction layer thickness

One of the most interesting results of this work comes from the parametric study through the electrode thickness (see Fig 12). Firstly, we noticed that the distribution of transfer current density is independent of the thickness of the electrode. This means that the part of the electrode that contributes to the reaction has a characteristic length which depends on several other parameters of the process. The objective of the demonstration that follows is to find an analytical expression for this characteristic length.

There are different methods to obtain the expression of the reaction layer thickness. The one presented here is the most rigorous. We started with the fact that the total charge exchanged during the electrochemical reaction is determined by the value of the inlet current density. This charge is exchanged from one conductor to another all over the cermet through the electrochemical reaction. Hence:

$$J_0 = \int_0^L \nu_e\, \varepsilon_{TP} i_r \mathrm{d}x \tag{69}$$

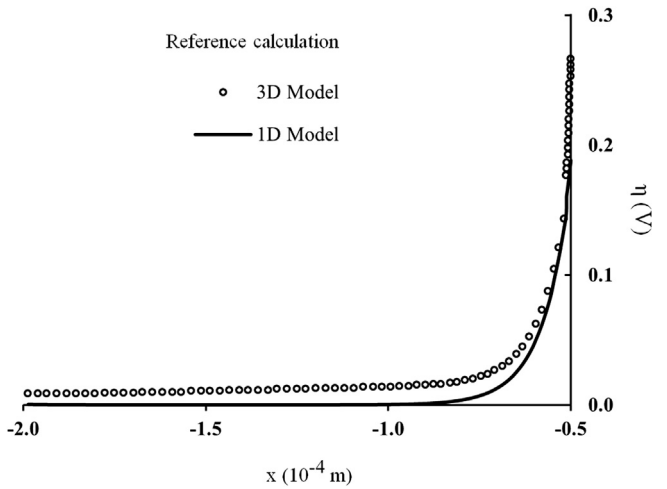

Fig. 8. Comparison between the two models on overpotential along the anodic cermet for the reference case. *X*-axis: position in the anodic cermet (on the left the anodic channel, on the right the electrolyte). *Y*-axis: overpotential.

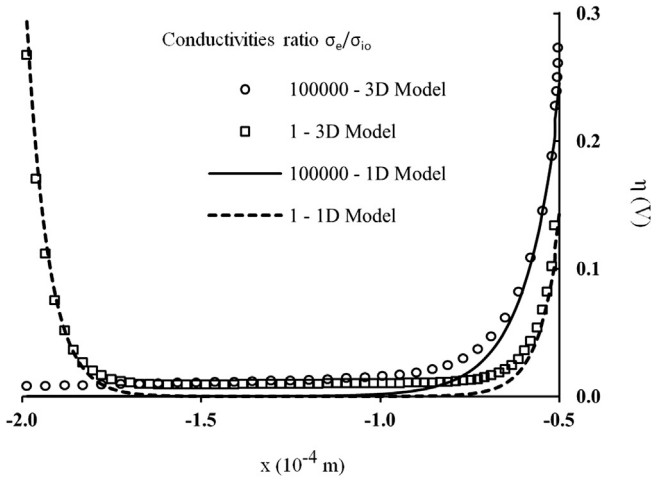

Fig. 9. Comparison between the two models on overpotential along the anodic cermet for different conductivities ratios. *X*-axis: position in the anodic cermet (on the left the anodic channel, on the right the electrolyte). *Y*-axis: overpotential.

We can define the reaction layer thickness, L_{reac}, as the portion of electrode in which 99.9% of this charge is exchanged.

$$\frac{999}{1000}J_0 = \int_{L-L_{reac}}^{L} \nu_e \varepsilon_{TP} i_r dx \tag{70}$$

The assumption presented in Section 2.4 on conductivities was then considered. Moreover, defining a reaction layer supposes that the electrochemical reaction is confined to an area close to the electrolyte, which is valid for values of $A >> 1$. Therefore the hyperbolic functions can be approximated as exponential functions:

$$\mathrm{ch}x \approx \mathrm{sh}x \approx \frac{\exp x}{2} \tag{71}$$

using Equation (71) for the integration of Equation (70) :

$$\frac{1}{1000} = \exp\left(-\sqrt{A}x^*_{reac}\right) \tag{72}$$

We can now use a normal logarithm:

$$L_{reac} = \frac{7L}{\sqrt{A}} \tag{73}$$

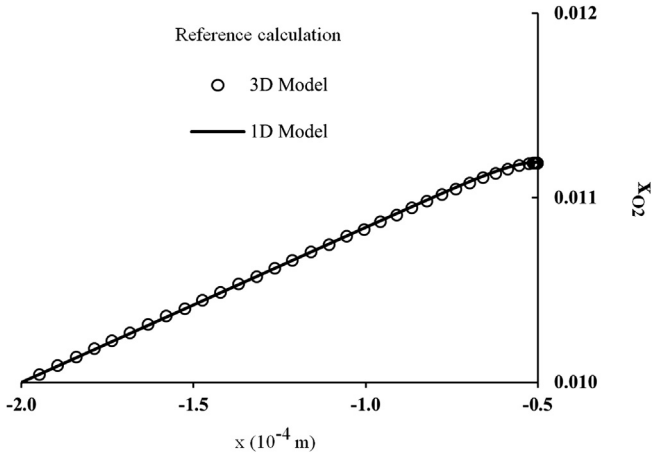

Fig. 10. Comparison between the two models on the molar fraction of oxygen along the anodic cermet for the reference case. *X*-axis: position in the anodic cermet (on the left the anodic channel, on the right the electrolyte). *Y*-axis: molar fraction of oxygen.

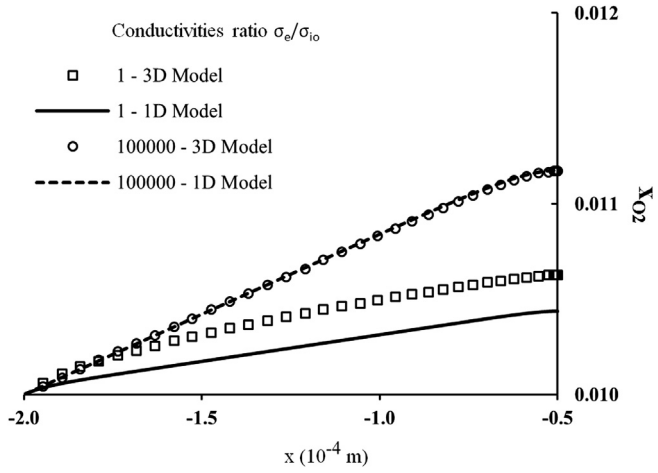

Fig. 11. Comparison between the two models on the molar fraction of oxygen along the anodic cermet for different conductivities ratios. *X*-axis: position in the anodic cermet (on the left the anodic channel, on the right the electrolyte). *Y*-axis: molar fraction of oxygen.

This expression is valid for $A > 50$. If $A < 50$, then $L_{reac} > L$ and defining a reaction layer is not possible.

In Fig 13, the reaction layer thickness is calculated and illustrated based on the results given by the model for the reference parameters. This graph clearly shows that the expression given in (72) for the calculation of the reaction layer thickness is relevant and accurate.

Two important comments can be made on this length. Firstly, it is not dependent on inlet current density and on the thickness of the electrode: as A is proportional to L^2, the ratio of L to the square root of A is independent of L, which confirms the results given in Fig 12. Away from this reaction zone, the electrode is inactive and this gives a valuable indication for the choice of its thickness. Secondly, L_{reac} depends on parameters of the process that are difficult to obtain experimentally such as exchange current density, i_r^0, or specific reactive volume, ε_{TP}. Therefore experimental determination of this length can help to determine those quantities. Note also that a quick parametric analysis can be made on L_{reac}, as A directly depends on the parameters of the process.

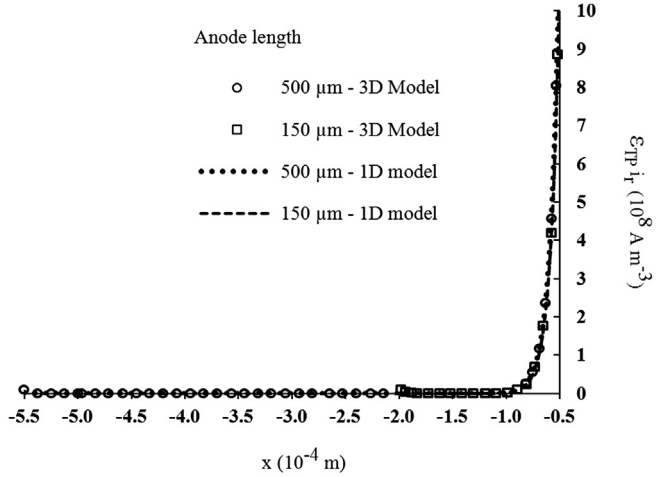

Fig. 12. Comparison between the two models on transfer current density along the anodic cermet for different electrode thickness. *X*-axis: position in the anodic cermet (on the left the anodic channel, on the right the electrolyte). *Y*-axis: transfer current density multiplied by the specific reactive volume.

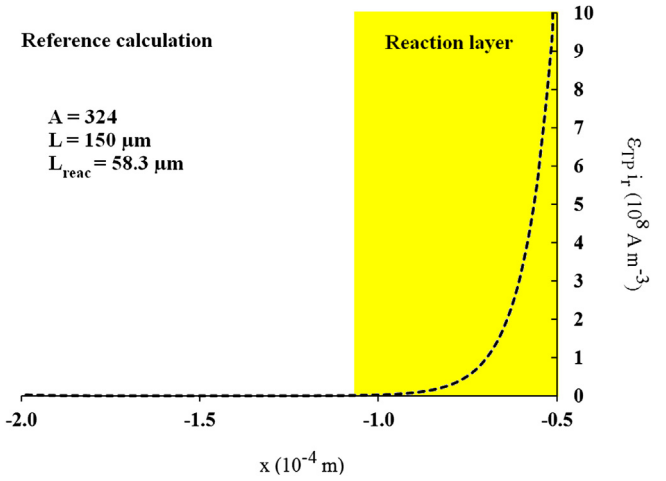

Fig. 13. Comparison between the two models on transfer current density along the anodic cermet for different conductivities ratios. *X*-axis: position in the anodic cermet (on the left the anodic channel, on the right the electrolyte). *Y*-axis: transfer current density multiplied by the specific reactive volume.

4. Comparison with results from the literature

The 1D model was compared with results from other studies on two scales:

- The macroscale level (I–V curves) where we compared the I–V curves given by the 1D model with experimental and correlated curves
- The microscale level, where we compared the results and models in literature for the estimation of the effective electrode thickness.

4.1. Macroscale level

For the macroscale level comparison, the expression of potential losses across the electrode assembly for the 1D model is required. It is obtained by adding the ohmic losses in the metallic and the ceramic phase by integrating Equations (24) and (25) using Equations (58) and (59) for each component of the assembly (anode, electrolyte, cathode).

$$\int_0^1 \sigma_0 \left(\frac{j_e^*(x^*)}{s_e \sigma_e} + \frac{j_{io}^*(x^*)}{s_e \sigma_e} \right) d_{x^*} = -\Delta\phi^* \tag{74}$$

The 1D model is then run and compared with the experimental results, using the data given by Meng Ni et al. [30] in Fig 14 (for proton conducting SOECs) and Y. Patcharavorachot et al. [31] (for proton-conducting SOFC) in Fig 15. The experimental conditions (i.e. operating conditions and electrodes properties) required for the calculation are usually not detailed enough on experimental studies, therefore the required data have been taken from the both previous studies cited above [30,31].

The 1D model shows good comparison with the experimental results and the correlations. On Fig. 14, the experimental results deviate from the models and experimental results given by Meng Ni et al. [30] for high current. However, the nonlinear behaviour of the experimental curve could be caused by an increased hydration of the ceramic due to higher steam fluxes in the electrodes, hence increasing the proton conductivity of the ceramic and therefore decreasing the ohmic losses in the ceramic. It is not the case in the models, where this proton conductivity is kept constant.

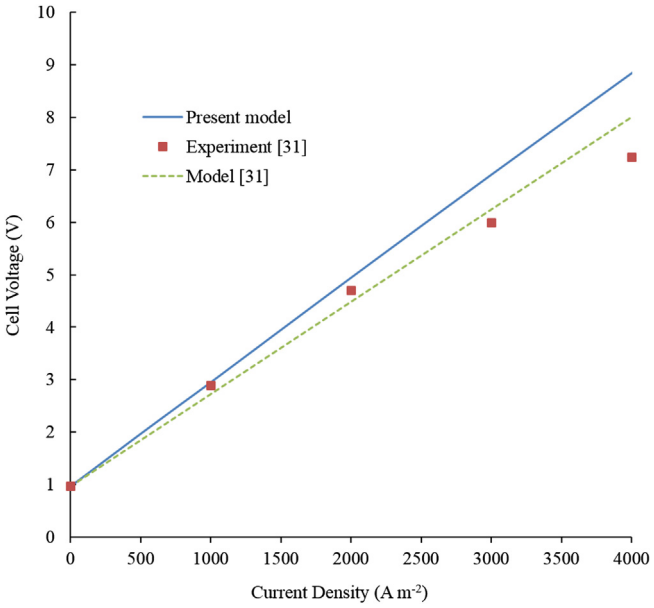

Fig. 14. Comparison between theoretical simulation results and experimental data given by Ni et al. [30].

4.2. Microscale level

Several experimental results and models can be found in literature on the effective electrode thickness of the reaction in a fuel/electrolysis cell electrode. The definition of the effective thickness varies from a study to another, however experimental results usually range the value of the effective thickness between a few microns to a few hundreds of microns, which is consistent with our study ($L_{reac} = 58$ µm). Lu et al. [32] and Fukunaga et al. [33] reported better cell performance with larger electrode assuming this was caused by a larger effective thickness. In our model though, the effective thickness remains independent of the electrode dimensions. It is not obvious to know which observation is right: this difference may either results from the deviation of the 1D model at high currents, or from the electrode properties varying during their preparation prior to the experiment. In addition, the correlation between a better performance and a larger effective thickness is not

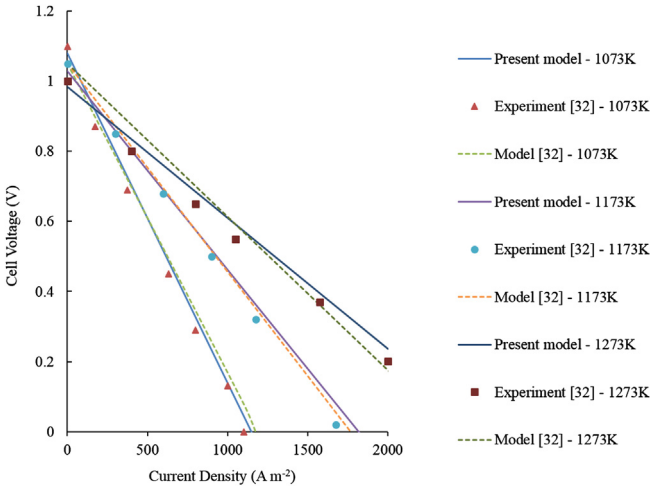

Fig. 15. Comparison between theoretical simulation results and experimental data given by Patcharavorachot et al. [31].

obvious. Some other studies also observed that the effective thickness vary with the value of the inlet current density, which again may be the case for high currents, where the 1D model is not valid anymore.

Models in literature are usually based on equivalent resistance modelling and present different expressions of the effective electrode thickness. These models are usually not derived from a set of equations and are built to extract the specific resistances of the systems by fitting experimental data.

Juhl et al. presented in 1998 a resistance model used for establishing the expression of the effective thickness as the ratio of the triple phase boundary resistance to the resistance of the ceramic [34]. The physical meaning of this expression is similar to the physical meaning of the A number presented in this study in Equation (62) and used for the calculation of the effective thickness in Equation (73). Juhl et al. also expected the effective thickness to increase with temperature, which is the case in our model. Shikazono et al. also noted that the effective thickness changed with gas composition, which is consistent with our study as well [35]. Finally, O'Hayre et al. [36] and Adler et al. [37] presented models where the value of the effective thickness decreases with an increasing exchange current density, which again is consistent with the model presented in this work.

It is however difficult to assess which expression is the most exact. On one hand, the model developed here was rigorously derived from a set of general equations for low currents but requires a lot of data to be checked experimentally. On the other hand, models currently reported in the literature are probably not comprehensive enough as they are built to fit the results given by the experiment of a single or a few studies. Although all of these expressions are approximate, including the one presented in this study, they tend to show the same dependencies, which is a good point. In addition they all predict values of effective thicknesses in the same range.

5. Conclusion

The analysis presented in this work is based on a differential equation system developed by Dumortier et al. [17] to model the transport processes inside solid oxide cells using a cermet. A set of assumptions based on the parameters of the system was established in order to linearize the complex differential system for low inlet current densities. By integrating the system, we established explicit functions relating the quantities of the process to the electrode properties and the position in the cermet. The functions show a good agreement with the values obtained with the non-linearized system. Characteristic dimensionless numbers were found by expressing the linearized system in a dimensionless form. Together with the system equations, we described a relevant dimensionless term, A, comparing the resistance of the electrode to charge transfer at the triple phase boundary and the electrical resistance of the metal and the ceramic to charge conduction. This dimensionless term was shown to be pertinent to the study of the distribution of the electrochemical reaction rate across the cermet. We also showed that the electrochemical reaction can be confined to a layer whose dimension is calculated with this number. The thickness of this layer does not depend on inlet current density or on the thickness of the electrode. It is therefore an indicator to optimize the thickness of the electrode. In addition, the layer has been explicitly formulated with the parameters of the process and the properties of the cermet. Consequently, the values of quantities that are difficult to obtain experimentally can be determined by experimental measurement of the layer. A comparison with experimental data and correlations from the literature on this effective thickness showed that our model is in good agreement with the current results on the matter.

Acknowledgements

The authors wish to thank the French ANR (National Agency for Research, France) for their financial support (Project ANR-09HPAC-007-01).

References

[1] B. Yildiz, M.S. Kazimi, Int. J. Hydrogen Energy 31 (2006) 77–92.
[2] C. Deslouis, M. Keddam, K. Rahmouni, H. Takenouti, F. Grasset, O. Lacroix, B. Sala, Electrochim. Acta 56 (2011) 7890–7898.
[3] X. Xue, J. Tang, N. Sammes, Y. Du, J. Power Sources 142 (2005) 211–222.
[4] R. Suwanwarangkul, E. Croiset, M.W. Fowler, P.L. Douglas, E. Entchev, M.A. Douglas, J. Power Sources 122 (2003) 9–18.
[5] M.M. Hussain, X. Li, I. Dincer, J. Power Sources 189 (2009) 916–928.
[6] J. Deseure, Y. Bultel, L. Dessemond, E. Siebert, Electrochim. Acta 50 (2005) 2037–2046.
[7] S. Kakaç, A. Pramuanjaroenkij, X.Y. Zhou, Int. J. Hydrogen Energy 32 (2007) 761–786.
[8] M.M. Hussain, X. Li, I. Dincer, J. Power Sources 161 (2006) 1012–1022.
[9] A. Pramuanjaroenkij, S. Kakaç, X. Yang Zhou, Int. J. Hydrogen Energy 33 (2008) 2547–2565.
[10] M. Ni, Int. J. Hydrogen Energy 34 (2009) 7795–7806.
[11] S. Murthy, A.G. Fedorov, J. Power Sources 124 (2003) 453–458.
[12] G. Wang, Y. Yang, H. Zhang, W. Xia, J. Power Sources 167 (2007) 398–405.
[13] M. Ni, Chem. Eng. J. 164 (2010) 246–254.
[14] S.A. Hajimolana, M.A. Hussain, W.M.A.W. Daud, M. Soroush, A. Shamiri, Renew. Sustain. Energy Rev. 15 (2011) 1893–1917.
[15] S. Authayanun, M. Mamlouk, A. Arpornwichanop, Int. J. Hydrogen Energy 37 (2012) 6808–6817.
[16] M. Ni, M.K.H. Leung, D.Y.C. Leung, Electrochim. Acta 52 (2007) 6707–6718.
[17] M. Dumortier, J. Sanchez, M. Keddam, O. Lacroix, Int. J. Hydrogen Energy 37 (2012) 11579–11594.
[18] E.L. Gyenge, J. Power Sources 152 (2005) 105–121.
[19] M. Grae Worster, M. Le Bars, J. Fluid Mech. 550 (2006) 149–173.
[20] W. Suksamai, I.S. Metcalfe, Solid State Ionics 178 (2007) 627–634.
[21] H. Hayashi, H. Inaba, M. Matsuyama, N.G. Lan, M. Dokiya, H. Tagawa, Solid State Ionics 122 (1999) 1–15.
[22] Y. Shi, N. Cai, Tsinghua Sci. Technol. 11 (2006) 701–711.
[23] J. Deseure, L. Dessemond, Y. Bultel, E. Siebert, J. Eur. Ceram. Soc. 25 (2005) 2673–2676.
[24] X.J. Chen, S.H. Chan, K.A. Khor, Electrochim. Acta 49 (2004) 1851–1861.
[25] Y. Ji, K. Yuan, J.N. Chung, J. Power Sources 165 (2007) 774–785.
[26] D. Chen, Z. Lin, H. Zhu, R.J. Kee, J. Power Sources 191 (2009) 240–252.
[27] P. Costamagna, P. Costa, V. Antonucci, Electrochim. Acta 43 (1998) 375–394.
[28] R.B. Bird, W.E. Stewart, E.N. Lightfoot, Transport Phenomena, John Wiley & Sons, New York, 2001.
[29] B.E. Poling, J.M. Prausnitz, J.P. O'Connell, The Properties of Gases and Liquids, McGraw-Hill, New York, 2004.
[30] M. Ni, M.K.H. Leung, D.Y.C. Leung, Int. J. Hydrogen Energy 33 (2008) 4040–4047.
[31] Y. Patcharavorachot, N.P. Brandon, W. Paengjuntuek, S. Assabumrungrat, A. Arpornwichanop, Solid State Ionics 181 (2010) 1568–1576.
[32] Z. Lu, J. Hardy, J. Templeton, J. Stevenson, J. Power Sources 198 (2012) 90–94.
[33] H. Fukunaga, M. Ishino, K. Yamada, Electrochem. Solid-State Lett. 10 (2007) B16–B18.
[34] M. Juhl, S. Primdahl, C. Manon, M. Mogensen, J. Power Sources 61 (1996) 173–181.
[35] N. Shikazono, D. Kanno, K. Matsuzaki, H. Teshima, S. Sumino, N. Kasagi, J. Electrochem. Soc. 157 (2010) B665–B672.
[36] R. O'Hayre, D.M. Barnett, F.B. Prinz, J. Electrochem. Soc. 152 (2005) A439–A444.
[37] S.B. Adler, J.A. Lane, B.C.H. Steele, J. Electrochem. Soc. 143 (1996) 3554–3564.